Diagnostic and Interventional Imaging (2013) **94**, 1187—1204

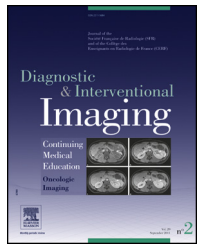

CONTINUING EDUCATION PROGRAM: FOCUS...

Perfusion and vascular permeability: Basic concepts and measurement in DCE-CT and DCE-MRI

C.A. Cuenod[a,b,*], **D. Balvay**[b]

[a] *Department of Radiology, Hôpital Européen Georges-Pompidou, Paris Descartes University, 20, rue Leblanc, 75015 Paris, France*
[b] *Imaging Research Laboratory (LRI), INSERM U970 HEGP Parcc (Paris-Centre de recherche Cardiovasculaire), 75015 Paris, France*

KEYWORDS
Perfusion;
Capillary permeability;
Angiogenesis;
DCE-CT;
DCE-MRI

Abstract The microvascular network formed by the capillaries supplies the tissues and permits their function. It provides a considerable surface area for exchanges between blood and tissues. All pathological conditions cause changes in the microcirculation. These changes can be used as imaging biomarkers for the diagnosis of lesions and optimisation of treatment. Among the many imaging techniques developed to study the microcirculation, the analysis of the tissue kinetics of intravenously injected contrast agents is the most widely used, either as positive enhancement for CT, T1-weighted MRI and ultrasound — dynamic contrast-enhanced-imaging (DCE-imaging) — or negative enhancement in T2*-weighted brain MRI — dynamic susceptibility contrast-MRI (DSC-MRI) —. Acquisition involves an injection of contrast agent during the acquisition of a dynamic series of images on a zone of interest. These kinetics may be analyzed visually, to define qualitative criteria, or with software using mathematical modelling, to extract quantitative physiological parameters. The results depend on the acquisition conditions (type of imaging device, imaging mode, frequency and total duration of acquisition), the type of contrast agent, the data pre-processing (motion correction, conversion of the signal into concentration) and the data analysis method. Because of these multiple choices it is necessary to understand the physiological processes involved and understand the advantages and limits of each strategy.

* Corresponding author. Department of Radiology, Hôpital Européen Georges-Pompidou, Paris Descartes University, 20, rue Leblanc, 75015 Paris, France.
E-mail address: ca@cuenod.net (C.A. Cuenod).

2211-5684/$ — see front matter
http://dx.doi.org/10.1016/j.diii.2013.10.010

The purpose of microcirculation imaging is to study blood flow in the capillary networks of the tissues [1—5] and the exchanges between the blood and the extravascular space [6,7]. It may be used at all stages of disease management for the early detection and characterization of a lesion and to provide a prognosis by determining severity factors. During recent years, this approach has been further developed in order to optimise treatments and monitor the clinical course of lesions during treatment [8—13].

Functional changes of the microcirculation occur before the morphological changes that are usually observed such as tumor growth for example [14] and provide quantitative results that may be used as imaging biomarkers [15] to assist decision-making.

Techniques to analyse the tissue microcirculation were originally developed in physiology [16—18] and nuclear medicine [19,20] and then, in the early 1980s, it was shown, based on the work of Meier and Zierler [21], that computed tomography (CT) could be used to study the microcirculation during the bolus injection of contrast agent [1]. However, acquisitions were long and restricted to a single-slice, which limited the performance of the technique. In addition, the fascination induced by the ever more precise visualization of anatomical structures by cross-sectional imaging overshadowed the interest of functional analysis.

Thanks to the development of MRI, the study of tissue perfusion has returned to the field of imaging [2,22—29].

It has now become possible to combine routine imaging of the microcirculation with morphological imaging, both by CT [12,30—32], IRM [9,33] or ultrasound [34]. This makes it possible to obtain morphological information with a high spatial resolution and functional information during a single examination. Tumor angiogenesis [35] is currently a subject of intensive study by functional imaging [36—44].

Several techniques for analyzing the microcirculation by cross-sectional imaging have been developed, but the most widely used strategy is the analysis of the kinetics of passage of a bolus of contrast agent through the tissues after a bolus intravenous injection. As the microcirculation is essential for all tissues, imaging studies can be conducted on all organs [45—61] and in a wide range of pathological conditions.

This article focuses on the strategy called dynamic contrast-enhanced-imaging (DCE) used to study the microcirculation by analyzing positive contrast enhancement in images [62]. The analysis can be performed both by MRI, CT or ultrasound, but the specific aspects of these different imaging methods developed in other reviews [63], will not be discussed here.

Characteristics and importance of the microcirculation

Overview

While the blood circulates in the large vessels (arteries and veins) at high speed that does allow exchanges with the tissues, the circulation in the microvasculature is very slow in order to permit exchanges between the blood and tissues: supply of oxygen, nutrients, heat, hormones and mediators, etc. and removal of products including CO_2, catabolites, toxins, heat, hormones and mediators, etc. (Boxed text 1). The term ''blood perfusion'', in the general sense, refers to the passage of blood through the microcirculatory network of an organ or tissue. The terms ''capillary permeability'' and ''capillary leakage'' refer to the passage through the capillary wall (considered to be a semi-permeable membrane), of a compound, which then diffuses into the interstitial space.

Boxed text 1 The main functions of the microcirculation.

1. Supply of oxygen and nutrients (including drugs and toxins)
2. Removal of CO_2 and other metabolic waste products (catabolites, toxins)
3. Release and capture of mediators (hormones, neurotransmitters, etc.)
4. Production of the immune response and inflammation
5. Regulation of tissue fluids (oedema)
6. Regulation of tissue temperature and core body temperature
7. Blood pressure control

Each tissue has a microcirculatory network with its own characteristics adapted to the specific function of the organ: e.g., continuous brain capillaries are almost impermeable to many substances, including iodinated and gadolinium-based contrast agents (blood-brain barrier or BBB), whereas in contrast, the hepatic sinusoidal capillaries, with their large fenestrae (pores) are highly permeable, including to macromolecules. In addition, pathological tissues have different microcirculatory networks than healthy tissues allowing them to be identified. For example, cancer tissues have capillary networks formed by ''neoangiogenesis'' in response to growth factors secreted by tumor cells such as the vascular endothelial growth factor (VEGF) [35]. These new and immature capillary networks have very different morphological and functional characteristics to those of the original healthy tissue.

Characteristics of the microcirculation

The microcirculatory network comprises vessels with a diameter of less than 200 μm. These are the arterioles, blood capillaries and venules as well as lymphatic capillaries and lymphatic collectors.

Capillaries are about 5—8 μm in diameter, whereas red blood cells have a mean diameter of 7 μm. Red blood cells circulate in single file through the capillaries and must sometimes be deformed in order to pass through smaller capillaries. An adult has about 100,000 km of capillaries with an estimated total surface area of 1000 m^2 (equivalent to about 3 tennis courts) over which exchanges take place. On leaving the capillary, the blood is collected by the venules with a diameter of 10 to 200 μm.

The microvascular vessel wall consists of a single layer of flattened cells or endothelial cells, forming the endothelium. This wall may be surrounded by a few contractile smooth muscle cells or pericytes. Exchanges of elements

contained in the blood and the extravascular space of tissues are governed by the endothelium. The smooth muscle cells can contract, reducing the diameter of the arterioles and capillaries, in order to regulate blood flow in this microcirculatory network.

Depending on their physicochemical characteristics (size, shape, polarity, etc.) blood components may cross the capillary wall by convection or transmembrane diffusion through pores and channels in endothelial cells, or via the junctions between endothelial cells, which are more or less tight depending on the type of capillary network. The impermeability of the BBB to most molecules is due to the presence of tight junctions between the endothelial cells of brain capillaries.

Physiological parameters of the microcirculation

Each tissue has a specific microvascular network and microcirculatory system of its own and many pathological processes (ischemia, inflammation, cancer, diabetes, etc.) can alter the architecture and system of this network. It is therefore useful to characterize the microcirculatory network by determining its physiological parameters in order to allow diagnosis and therapeutic monitoring.

Microcirculatory parameters are generally expressed for a given mass or volume of tissue so that different tissues can be compared. As in cross-sectional imaging a voxel represents one volume element of tissue, the parameters of the microcirculation (Fig. 1) are expressed per unit of volume.

Tissue blood flow

The tissue blood flow (F_T) corresponds to the blood flow entering (and exiting) a volume of tissue (expressed in mL of blood/min/100 mL tissue). For example, for the brain we use the term cerebral blood flow (CBF). Tissue blood flow is often referred to by the short and ambiguous term ''perfusion''.

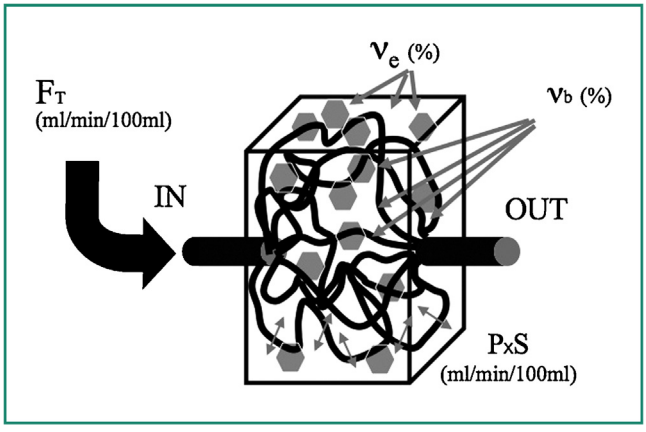

Figure 1. Main parameters of the microcirculation: the quantity of blood that arrives per unit time in the vascular network in a volume element of tissue (voxel) corresponds to the tissue blood flow (F_T); the volume of blood contained in the capillaries of the voxel corresponds to the blood volume fraction (ν_s); the interstitial volume corresponds to the extravascular and extracellular volume fraction (ν_e); the leakage rate through the capillary walls is measured by the surface permeability × total surface area of the capillary walls contained in the voxel (P × S). Hexagons symbolize cells.

Tissue blood volume (BV_T) or blood volume fraction (ν_b)

The tissue blood volume (BV_T) or blood volume fraction (ν_b) corresponds to the volume of capillary blood contained in a certain volume of tissue. This ratio is expressed in mL blood/100 mL of tissue or in %. For example, for the brain we use the term cerebral blood volume (CBV). The tissue blood volume is often referred to by the misnomer ''blood volume''.

Mean transit time (MTT)

The MTT is the mean time taken by blood to pass through the capillary network (time between the arterial inflow and venous outflow) (expressed in second).

Permeability—surface area product

The permeability—surface area product (P × S often written PS) is the flow of molecules through the capillary membranes in a certain volume of tissue (expressed in mL/min/100 mL tissue). PS depends not only on the characteristics of the capillary wall, but also the contrast agent used. PS is sometimes called Ktrans, but in fact the PS only corresponds to Ktrans under very specific conditions.

Transfer constant Ktrans

The transfer constant Ktrans is a complex combination of tissue blood flow and PS in varying proportions depending on the circulatory system and measurement conditions [64].

Extravascular and extracellular volume fraction (ν_e)

The tissue interstitial volume or extravascular and extracellular volume fraction (ν_e) is the interstitial volume, i.e. extravascular and extracellular volume contained in a volume of tissue, and in which extracellular contrast agents may accumulate if they cross the endothelial barrier (expressed in mL of extravascular extracellular volume/100 mL of tissue or %). The distribution volume is often called the ''extravascular extracellular space'' (EES).

The parameters of the microcirculation and the variables of interest used to calculate them are listed in Table 1.

Notes regarding the parameters of microcirculation

Note 1

The blood flow in a large vessel is measured by a flow rate Q (quantity or volume of blood passing through a tube of given surface area) expressed as volume of blood per unit of time (for example in mL/min), and can be determined using Doppler ultrasound by multiplying the blood velocity (V) in the vessel by the cross-sectional area (S) of the vessel $Q = V \times S$. However, the blood flow in a tissue is measured by ''flow per tissue volume'' (tissue blood flow), expressed as a volume of blood per unit time and per unit volume of tissue (mL/min/100 mL).

Table 1 Quantities of interest. The unit volume of tissue is expressed per 100 mL rather than grams as cross-sectional imaging devices provide data on tissue volumes. The use of mL overcomes the problem of conversion by density (ρ), which may be unknown for the tissue of interest (lung parenchyma, bone, etc.).

Quantity	Definition	Unit
Cab	Tracer concentration in the arterial blood	mM
Cap	Tracer concentration in the arterial plasma	mM
Ctp	Tracer concentration in the tissue plasma	mM
Cvp	Tracer concentration in the venous plasma	mM
Ce	Tracer concentration in the interstitium	mM
Ct	Tracer concentration in the tissue	mM
Cvb	Tracer concentration in the venous blood	mM
Cvp	Tracer concentration in the venous plasma	mM
E	Initial extraction fraction	None (%)
Hct	Hematocrit: Ca = (1-Hct)Cp	None (%)
Ft	Perfusion or blood flow rate per unit volume of tissue	mL/min/100 mL
Ftp	Perfusion or plasma flow rate per unit volume of tissue	mL/min/100 mL
P	Permeability per unit surface area of capillary wall	cm/min
S	Surface area of capillary wall per unit volume of tissue	cm^2/100 mL
P × S	Permeability—surface area product per unit volume of tissue	mL/min/100 mL
Ktrans or EFp	Constant volume transfer or extraction fraction × or plasma perfusion rate	mL/min/100 mL
Vb	Total volume of blood	mL
Ve	Total volume of interstitium	mL
Vp	Total volume of plasma	mL
ν_s	Blood volume fraction per volume of tissue	None (%)
ν_p	Plasma volume fraction per volume of tissue	None ()
ν_e	Interstitial volume fraction per volume of tissue	None (%)
MTT	Mean transit time	s
HPI	Hepatic perfusion index: arterial infusion/total infusion	%

Adapted from the standardization article [23].
s: second.

Note 2

It is possible to express F_T in min^{-1} or s^{-1} by cancelling the mL in the numerator and denominator, but it is important to keep the mL in the expression ''mL/min/100 mL'' as a reminder that the numerator is mL of blood and the denominator mL of tissue.

Note 3

Flow and volume parameters can be measured as a function of plasma rather than blood. The parameters analyzed are then the tissue plasma flow (expressed in mL plasma/min/100 mL of tissue) and tissue plasma volume (expressed in mL plasma/100 mL of tissue). The correspondence between the parameters expressed for plasma and those expressed for blood involves the hematocrit (Hct), which is the relative percentage in volume of red blood cells circulating in the blood relative to the total blood volume (about 45%) (Table 1).

Note 4

The mean transit time (MTT) can be calculated as the ratio between the tissue blood (or plasma) volume and the tissue blood (or plasma) perfusion rate: $MTT = \nu_s/F_T$ according to the ''central volume'' theory of Stewart and Hamilton. Consequently, if one of the parameters ν_s or F_T is known in addition to MTT the other parameter can be calculated.

Note 5

While the tissue blood flow and blood volume parameters are constant for a capillary network at any given time and are not influenced by the type of contrast agent used, there is a specific value of the parameter PS (permeability—surface area product) for each contrast agent used. This accounts for the fact that a small or lipophilic contrast agent passes more easily through the endothelial wall of the capillaries than a larger or hydrophilic contrast agent. Extremely large agents such as the bubbles used in ultrasound, with diameters of between 1 and 10 mm, do not pass through the capillary membrane. Similarly, the conventional contrast agents used in CT and MRI do not pass through the blood-brain barrier when this is intact, and the measurable PS for these contrast agents is zero: analytical models are simplified when there is no interstitial leakage to take into account.

The main quantities used in the study of the microcirculation and their units are summarized in Table 3.

Methods of measuring the microcirculation

Methods for measuring the microcirculation other than imaging

Because of the importance of the microcirculation in medicine, many techniques have been developed for its

study. Each technique has its own limitations. Some only allow the study of specific superficial tissues such as capillaroscopy, retinal angiography, laser Doppler flowmetry (LDF) [65] or plethysmography; others are invasive such as the use of isolated perfused organs or autoradiography and require tissue samples or the sacrifice of animals, intravital microscopy [66,67] or flow measurement by thermal diffusion, etc. Most of these techniques only provide semi-quantitative data making it difficult to distinguish specific physiological phenomena. For example, because of uncertainties about the measurement volume in which circulating red blood cells are detected by laser Doppler, the results do not represent a flow, but a ''tissue perfusion index'' dependent both on the red blood cell velocity and their local concentration.

Methods for measuring the microcirculation by cross-sectional imaging

Cross-sectional imaging techniques have many advantages for the study of the microcirculation, and in particular, they permit the noninvasive investigation of deep structures *in vivo* and can be coupled with a morphological study.

History

Since the introduction of contrast agents, the microcirculation has proved to be an important part of the diagnostic imaging strategy because of differences in tissue enhancement after their injection. The terms ''hypervascular'' and ''hypovascular'' tissue are commonly used in radiological reports, although these tissue enhancements are the end result of several different factors (density of the capillary network, blood concentration of contrast agent, extravasation of contrast into the interstitial space, etc.) that cannot be separated on static images. The acquisition of images at specific times after injection (arterial, portal or late phases) has led to an improvement in the detection and characterization of lesions, taking into account the microcirculatory characteristics of tissues, such as in hepatic hemangiomas [68].

Functional analysis of microcirculatory phenomena was originally developed in nuclear medicine [19], but there were then limitations due to the lack of cross-sectional imaging (resulting in the superimposition of tissues with different characteristics). Currently, this limitation has disappeared with tomography techniques (PET and SPECT), although the low spatial resolution limits the accurate measurement of the arterial reference, making it necessary to take arterial blood samples.

Several methods for the analysis of the microcirculation by cross-sectional radiological imaging have been developed by adapting the principles used in nuclear medicine. The first publications date back to the 1980s with CT scan acquisitions [1]. At that time, scanners had long acquisition times and only a small region could be examined. This analysis was then developed by MRI, thanks to the many techniques offered by the multiparametric nature of this technique and the absence of radiation, before further progress was made by CT [30] with multidetector-row helical acquisition [69] followed by Dual Energy CT [70] and dose-reduction techniques [71]. The analysis of the microcirculation by ultrasound has also developed with the introduction of bubble-based contrast agents [72,73].

Large panel of MRI methods

There are many strategies, in particular in MRI, to analyse the microcirculation, such as intravoxel incoherent motion (IVIM) imaging where pseudo-diffusion measured at low b-values is used to estimate a circulating volume fraction [2], arterial spin labelling (ASL) [74,75] during which the circulating blood is magnetically labelled, and recently the combination of ASL with diffusion [76]. Blood oxygen level dependency (BOLD) imaging [77] may also be mentioned where the ratio of oxygenated haemoglobin and paramagnetic deoxygenated haemoglobin [78] provides an indirect analysis of the tissue oxygen supply [79].

However, the most commonly used approach is the analysis of the kinetics of passage of a bolus of contrast material through the tissues. When positive enhancement is used (T1 effect by MRI and signal enhancement on CT or ultrasound), the technique is called ''dynamic contrast-enhanced-imaging'' DCE-imaging. DCE-imaging is used in CT and US for all anatomical regions and in MRI for regions outside the brain. When negative enhancement is used (signal drop, due to the susceptibility effects induced by the first-pass of the bolus of concentrated contrast agent with T2/T2*-weighted MRI sequences), the technique is called dynamic susceptibility contrast-MRI (DSC-MRI); this was the first technique used historically [22] and is currently used for brain MRI. Strictly speaking, DSC-MRI cannot be used to investigate capillary leakage and its analysis theoretically implies that the blood-brain barrier is intact and impermeable to contrast agents.

Tissue kinetics of contrast agents or DCE-imaging

General principle of DCE-imaging

DCE-Imaging is the method most commonly employed for imaging studies of the microcirculation in tissues other than the brain. Its principle consists in injecting a contrast agent during the repeated acquisition of images on a same (or several) slice(s) and collecting the signal enhancement kinetics in the tissues (Fig. 2). The temporal kinetics of enhancement depends on the local circulatory system, the mode of injection (injection rate, dose, concentration of contrast agent) and type of contrast agent. It can be analyzed using different strategies to obtain visual criteria, semi-quantitative criteria or better, microvascular physiological parameters. It can be performed by each imaging modality and is referred to as DCE-CT, DCE-MRI and DCE-US.

Mechanisms involved in tissue enhancement kinetics after injection of contrast agent

In order to master the principles of DCE-imaging and not be misled by the often complex and sometimes imprecise publications in the literature, it is necessary to understand the basic phenomena involved in the kinetics of tissue enhancement. Two essential phenomena occur simultaneously:

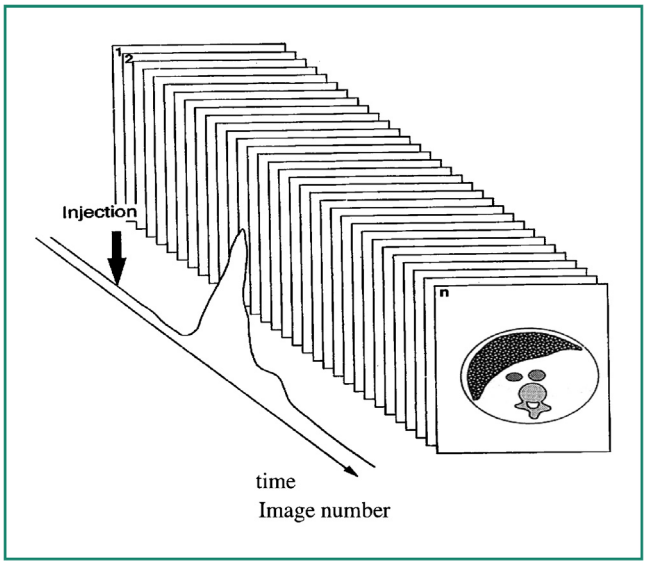

Figure 2. Sequential acquisition dynamic contrast-enhanced-imaging: a sequential acquisition is performed at the level of a slice or volume during the injection of contrast agent. Acquisition must begin before the start of injection to obtain reference images without contrast agent (baseline). Acquisition then continues after the injection.

perfusion in the microcirculatory network and accumulation in the interstitium followed by release from the interstitium due to capillary leakage. These two phenomena have different time courses and kinetics but they overlap, leading to a potential source of confusion.

Pure tissue perfusion

During pure tissue perfusion (without interstitial leakage) (Fig. 3a) the behavior of a molecule of contrast agent can be artificially divided into three phases (Fig. 4a):

- entry into the capillary network from the arterial system;
- followed by circulation in capillary network;
- finally exit into the venous network.

As all the molecules of contrast agent do not enter the capillary network at exactly the same time, the enhancement slope tells us about the tissue perfusion flow (Fig. 5-1). This phenomenon is very fast and can only be reliably recorded if the image acquisition speed itself is very rapid (less than 3—5 seconds per image). When the capillaries

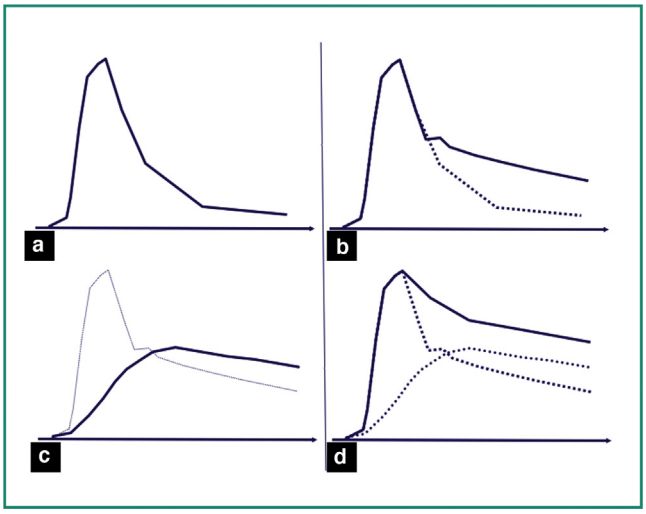

Figure 4. Tissue enhancement after bolus injection of contrast agent: a: if the contrast agent remains confined in the microvascular network and if it is completely eliminated by the kidneys during the first passage, tissue enhancement would show a rapid rise after the arrival of the bolus, followed by a rapid exponential decay to a value close to the initial value before the injection; b: as the contrast is not immediately eliminated, the second part of the signal decay is much slower due to the recirculation of contrast agent (solid line). The second passage is sometimes visible as a second peak, which is much lower than the first peak; c: in case of leakage through the capillary wall, accumulation of contrast agent in the interstitium is added, with slower kinetics and the contrast agent is only eliminated later from the interstitium when the concentration of contrast agent in the plasma becomes lower than that in the interstitium (solid line). The interstitium has a reservoir effect (capacitance); d: finally, the tissue enhancement (solid line) is the sum of the enhancement induced by the presence of contrast agent in the capillary network plus the enhancement induced by the presence of contrast agent in the interstitium (dotted lines).

are filled with blood containing the maximum concentration of contrast agent, and before they start to empty, the maximum (peak) enhancement informs us about the blood volume fraction (provided there is no interstitial leakage) (Fig. 5-2).

After reaching a peak, the enhancement rapidly decreases during the evacuation of the molecules of contrast agent derived from the bolus: the contrast agent recirculates and is slowly eliminated (Fig. 4b) by renal filtration.

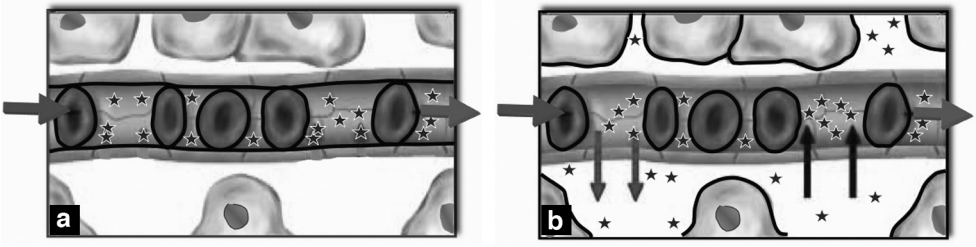

Figure 3. Distribution of the contrast agent in a volume of tissue, according to the type of contrast agent and type of tissue: a: the red cell membrane and the capillary endothelial cell membrane are impermeable to the bubbles used for ultrasound imaging and iodinated or gadolinium-based contrast agents used in the brain (BBB). The contrast agent (stars) remains confined in the blood plasma; b: contrast agents in the blood can diffuse into the interstitium through the endothelial wall of the capillaries and then return back to the blood. Iodinated and gadolinium based contrast agents does not enter into the cells.

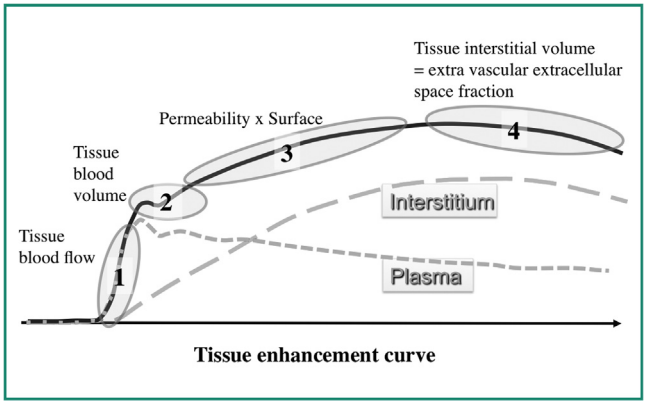

Figure 5. Significance of different parts of the tissue enhancement curve: the tissue enhancement (continuous curve) is the sum of the plasma component (small dots) and the interstitial component (large dots). The first part of the curve (1 rapid rise) mainly depends on the tissue perfusion flow rate, the early peak (2) depends on the tissue blood volume, the part after the peak (3) depends on leakage into the interstitium and the later part (4) depends on the tissue interstitial volume and the return of the contrast agent into the blood compartment.

Leakage of the contrast agent into the interstitium

If the capillary wall is permeable to the contrast agent (Fig. 3b), the leakage of the contrast agent into the interstitium is proportional to the difference in concentration of contrast agent between the blood plasma and interstitium on both sides of the capillary wall (according to Fick's first law). In other words, as the concentration is higher in the plasma than in the interstitium, there are more contrast agent molecules which penetrate into the interstitium across the endothelial wall than molecules contained in the interstitium that return to the plasma: the net result is an accumulation of contrast agent molecules in the interstitial tissue (Fig. 4c). The accumulation rate is proportional to the difference in concentration of contrast agent across the capillary wall (or concentration gradient), the permeability (P) of this wall to the agent and the total surface area (S) of capillary walls contained in the tissue. The rapid initial slope of enhancement induced by the perfusion is combined with a slower slope induced by the interstitial accumulation of contrast agent (Fig. 5-3).

Then, from the time when the plasma concentration due to renal excretion becomes lower than the interstitial concentration, the balance of flow of contrast agent across the capillary membrane changes direction and the interstitium is gradually emptied of molecules of contrast agent. The decrease in signal corresponding to this release is then combined with the purely vascular declining slope. Its kinetics provides information about the tissue interstitial volume fraction (Fig. 5-4).

The phenomenon known as ''late enhancement'' conventionally used to identify fibrotic lesions (cardiac infarction scar, cholangiocarcinoma, ovarian fibroma, etc.) [80,81] corresponds to a progressive and significant accumulation of contrast agent in the large interstitial spaces contained within the fibrosis.

Finally, the net tissue enhancement visible on the images is the sum of the two phenomena of tissue perfusion and interstitium accumulation/release (Fig. 4d and Fig. 5). However, as the chronology and kinetics of tissue perfusion and leakage are different, it is possible to separate and analyse them individually by appropriate mathematical modelling.

Application of DCE-imaging — concepts common to all DCE-imaging techniques

Although they all come under the same general term of ''DCE-imaging'', the data acquisition and analysis protocols are actually very heterogeneous. This heterogeneity in practice is a source of confusion, which slows down the spread and the acceptance of DCE-imaging. Protocols mainly depend on four major components:

- the acquisition strategy, with as fundamental parameters the temporal resolution of acquisition, the total acquisition time of the sequence and the injection mode (injection rate, dose and concentration of contrast agent);
- the type of contrast agent (agent diffusible in the interstital space for CT and MRI, and microbubble-based blood pool agents for ultrasound);
- the data pre-processing (motion corrections and conversion of the signal into concentration);
- the analysis mode (from purely visual techniques to highly sophisticated mathematical modeling). The analysis can be performed on regions of interest (ROI), groups of voxels or individual voxels.

Protocols vary according to the practices of the imaging centres, the technical means at their disposal and organ specialties. In 3D dynamic contrast-enhanced MRI of the breast, for example, the acquisition of each volume is long (about 1 minute), the total acquisition time is also long (follow-up for 8 to 10 minutes) and the analysis is often visual, based on the overall shape of the enhancement and the more or less rapid decrease in the signal (washout), while conversely, much faster acquisition is used for cardiac perfusion imaging, (temporal resolution of one image every 1 to 3 seconds) over a very short total acquisition period (40 to 60 seconds) during the first-pass of the bolus of contrast agent and the quantitative parameters of cardiac blood flow and blood volume may be extracted by mathematical modelling.

Acquisition

The acquisition mode is of critical importance in DCE-imaging. The acquisition parameters must be adjusted according to the organ studied and the clinical setting. They directly affect the phenomena observed and the accessible microcirculation parameters. There are many possible protocols, making it difficult to compare different publications. Therefore, a certain form of standardization is necessary. The following parameters must be set:

- temporal resolution of the acquisition;
- total measurement time;
- single-slice, multi-slice or 3D acquisition mode;
- injection of contrast agents — method of injection: bolus, slow infusion — and volume and concentration of contrast agent;
- flushing with saline, or not.

It should be remembered that after the injection of a contrast agent, the very first times of tissue enhancement (Fig. 5) are dependent on the tissue perfusion rate; thereafter, the extravasation of the contrast agent may become of paramount importance. Perfusion will determine the arrival of the contrast agent in the tissues and the filling of the capillary network; this phenomenon is fast, occurs as soon as the bolus arrives, and requires a very high acquisition speed in order to be analyzed. On the contrary, leakage of the contrast agent and its interstital accumulation/release are slower phenomena requiring a long acquisition time for their analysis.

Mode of analysis

Note: it is of utmost importance to acquire several images prior to the beginning of contrast injection (at least 5 images, ideally 10) to get a reference baseline that is used to accurately quantify the enhancement (Fig. 2).

Contrast agents

The choice of contrast agent is currently limited in clinical practice to the ''extracellular diffusion'' agents authorised in humans for clinical use (small molecules in CT and MRI, diffusing into the interstitial spaces and with rapid renal clearance). Many other contrast agents are available for research, including macromolecular agents [82—90] and particulate agents such as iron oxides [91—93]. Use of macromolecular or particulate agents makes it easier to analyse the intra-capillary flow component by restricting the leakage rate into the interstitial fluid. These agents may also be used to analyse the leakage of large components, which is considered to be more specific of the tumor neovasculature than the leakage of small molecules.

The use of bubbles by ultrasound has the advantage that it overcomes capillary leakage phenomena, as the bubbles remain strictly within the vascular system, simplifying analysis and making it more robust. On the other hand, bubbles cannot be employed to measure and analyse capillary permeability.

Preconditioning of data

It is sometimes necessary to precondition data before performing the analysis stage. This mainly comprises correction of motion artefacts, noise suppression and conversion of the signal into contrast agent concentration.

Motion correction

The occurrence of movements during dynamic acquisition is a major problem that could lead to poor quality of DCE-imaging kinetics. These may be voluntary or involuntary movements of the patient despite restraining methods, but also physiological movements (breathing, heartbeat, and peristalsis). The need for precise temporal sampling generally rules out the use of synchronization techniques and the total acquisition time (sometimes several minutes) precludes breath holding. A motion correction process is needed to improve the quality of results. This may involve rigid registration techniques [94], although these cannot take into account the deformations of organs during movements, or non-rigid registration techniques [95]. Registration in DCE-imaging is tricky as the series can be long (with large movements), but mainly because the signal changes during time due to the kinetics of the contrast agent [96,97]. It is often easier to perform a localized registration (e.g. on a tumour, kidney or the heart) than trying to perform registration on the whole acquisition volume.

Noise filtering

DCE-imaging data generally have a low signal to noise ratio as acquisitions are rapid. However, as the data are highly correlated because of the enhancement kinetics, it is possible to use filter methods, in particular by using principal component analysis [98].

Conversion of the signal into concentration

To perform quantitative analyses using enhancement curves, it is necessary to calculate the equivalence between the enhancement values of a voxel at any time and the concentration of contrast agent present in this voxel.

This is directly performed by a CT-scanner, as the attenuation measured in Hounsfield units is proportional to the iodine concentration. However, the problem is much more difficult with MRI as the signal if affected by many phenomena: T1 relaxation, T2 and T2* relaxations, entry-slice phenomena, etc. Many strategies have been developed to minimise this problem including the use of saturation bands, T1 mapping [99—101], optimisation of the dose and concentration of injected contrast agent [102], optimisation of the flip angle [103,104], multi-echo acquisition [105], etc. The subject is complex and beyond the scope of this article.

Data analysis

Overview

The analysis of tissue enhancement curves can be performed on regions of interest (ROIs) on groups of pixels with similar kinetics (clusters) or voxel-by-voxel. It may be qualitative, semi-quantitative or quantitative. Visual qualitative analysis is the simplest, but quantitative analysis provides access to the functional parameters of the microcirculation making it possible to compare different patients or the same patient at different times in order to evaluate the effectiveness of treatment.

Softwares dedicated to the analysis of DCE-imaging sequences are becoming available to perform these analyses. This software is either included in manufacturers' workstations or developed in research laboratories. The continuous improvement of these computer programs offers a simpler and more rapid and robust analysis of the microcirculation.

Modes of analysis of enhancement kinetics

Qualitative or visual analysis. Enhancement kinetics can simply be analyzed visually on the native images or on images after subtraction of the image acquired before contrast injection, as for breast MRI (Fig. 6), focusing mainly on the speed of the filling phase (wash-in), peak intensity after this filling phase (peak), and the kinetics following this first phase (rapid decrease or washout, plateau or slow continuation of accumulation) [106]. This mode of analysis is very simple and rapid. It is effective for the characterization of certain tumors, in combination with morphological criteria. However as it does not give numerical results it is impossible to compare different patients or measure the effectiveness of treatment in the same patient.

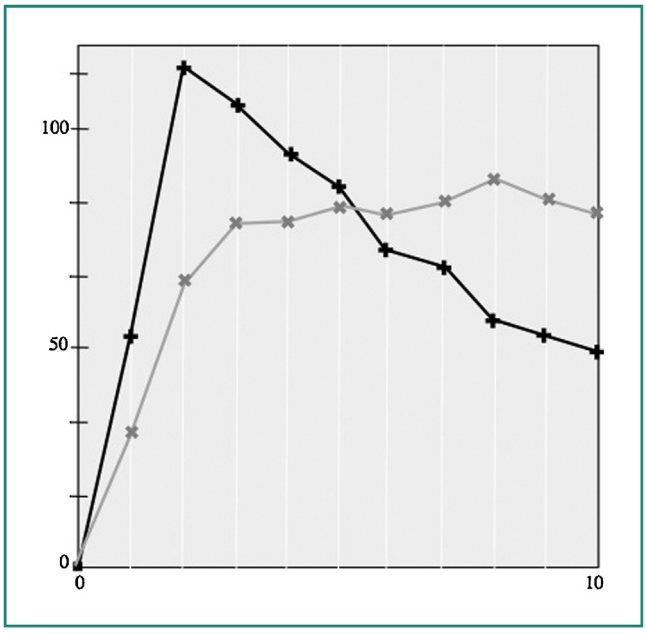

Figure 6. Visual analysis — breast MRI: a simple visual analysis shows that the black curve rises rapidly after injection with a peak on the acquired image after 2 min (rapid wash-in) and rapid descent (fast washout), while the grey curve rises more slowly (slow wash-in) to reach a plateau that persists during the observation period. The first kinetics is usually seen in cases of malignancy whereas the second kinetics is generally observed in the case of a benign tumor.

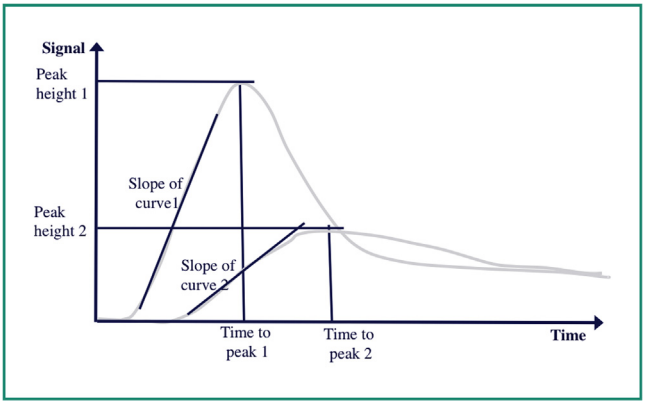

Figure 7. Semi-quantitative description without a model of the tissue enhancement curves. Two tissues are compared on this graph, the peak height of curve 2 is less than that of curve 1, the time to peak is longer for curve 2 and the slope of curve 2 is lower than that of curve 1. This analysis is simple and rapid although it may be hampered and subjective if the curves are noisy as it is then difficult to define the summit of the peak. This type of analysis is useful when it is possible to use an internal reference (e.g. contralateral brain or myometrium). In the above example obtained by a perfusion scan of the brain from two symmetrical insular regions of interest, curve 2 corresponds to an area of ischemic brain after an acute stroke, and curve 1 corresponds to the contralateral normal brain used as reference.

Computers can be used to automate the shape-recognition process of the enhancement for each pixel in order to create enhancement maps and detect areas of interest (e.g. hypervascular areas) in the images [107]. A method known as ''three time point analysis'' was developed to automatically characterize wash-in and washout behavior in breast MRI [108,109].

Semi-quantitative analysis (without a physiological model). Semi-quantitative parameters without model. Several descriptive or ''heuristic'' parameters can be analyzed from the tissue enhancement curve (Fig. 7), such as the slope of filling (maximum slope), the maximum enhancement (peak height) that can be expressed in % and the time to peak. The washout slope is generally more difficult to measure.

Semi-quantitative parameters with heuristic models. Descriptive parameters can be affected by the instability of the curves due to the presence of noise and motion in the images. Use of a purely descriptive (or heuristic) mathematical model to fit the curve provides a more precise definition of the parameters [110].

Area under the curve. The area under the curve (AUC), i.e. the integral under the enhancement curve, is a commonly used parameter, as it is more robust to noise and does not require a mathematical model [111]. The area under the curve can be measured during the early period (e.g. 90 seconds) and it is then called the initial area under the curve (IAUC).

Relative semi-quantitative parameters. The raw semi-quantitative parameters do not take into account the intra-arterial kinetics of the contrast agent although this can be very different in each patient depending on the injection protocol (volume, concentration, speed, etc.) and physiological conditions of the subject. They can be normalized by comparing them with those of a reference tissue such as muscle, the myometrium or a portion of the same tissue recognized to be non-pathological (e.g. the contralateral brain to a lesion as on Fig. 7) or even to the arterial enhancement curve. This normalization is performed by calculating ratios in order to obtain relative parameters. For the area under the curve, for example, the term relative AUC (AUCr) is used.

Arterial input functions

Quantitative analysis is performed using mathematical models that take into account the enhancement kinetics of the artery supplying the area studied (Table 3). By taking the arterial supply into account, it is possible to obtain representative quantitative parameters that can be compared from one patient to another or for the same patient between two examinations. Theoretically, the parameters obtained by DCE-imaging should be independent (within certain limits) of the injection mode and the patient's physiological status. These models mainly focus on studying the perfusion rate [1,5,112], capillary permeability [6,7,20,24,26,113,114], or both [89,90,115—125].

Tofts-Kety model. Originally developed by Tofts and Kermode for the study of multiple sclerosis [6], the Tofts model is currently the model most widely used in studies and is generally recommended in consensuses [126]. Although it does not give results that precisely correspond to a physiological reality, the results are robust as only two parameters are used to fit the enhancement curve. This model makes it possible for a centre, with identical acquisition conditions, to obtain reproducible and similar results.

It is nevertheless necessary to know its limitations and not give it a physiological interpretation or make

comparisons between centres not using exactly the same procedure.

This model only has two fitting parameters Ktrans and ν_e. It describes the entry of the contrast agent in the tissue without distinguishing between entry into the capillary network and entry into the interstitium. The transfer coefficient, Ktrans is an unknown combination between the tissue perfusion flow rate and PS, which varies according to physiological conditions and the conditions of acquisition [23,64]. The blood volume fraction is considered to be negligible, which is realistic in the brain with a blood volume fraction of 3 to 5%, but unrealistic in tissues such as the liver or tumours, which may have a blood volume fraction of 30 to 50%. The measured νe therefore corresponds to a combination of νe and νs also in unknown proportions. To overcome this limitation the extended Tofts-Kety model has been developed. It uses therefore three parameters which are Ktrans, ν_e and ν_s, leading to more realistic results at the expand of less robustness [159].

This model is not suitable for analyzing data acquired with a rapid temporal resolution, as the use of only two parameters generally does not allow a satisfactory fit of the first part of the curve with rapid kinetics.

Finally, the results are very dependent on the mode of acquisition [127] and cannot be used for comparisons between centres using different acquisition protocols.

Physiological models. There are many strategies (Table 2) that consist in performing a pharmacokinetic analysis based on modelling of tissue compartments.

The first models were developed to analyse the first passage of contrast agent at high temporal resolution, in order to assess tissue perfusion, or to study the later state of dynamic equilibrium at low temporal resolution, to assess interstitial leakage. Recent models take into account all the parameters of the microcirculation. These models are derived from a general formula taking into account exchanges between the arterial blood, the plasma and the interstitial space in which the parameters not available in the data are ignored by the model. A very precise general review on this subject has been published by Sourbron and Buckley [128].

The general formula for a two-compartment model (Fig. 8), where, to simplify, the capillary compartment and interstitial compartment are considered to be homogeneous, can be defined at any time (t) for a unit volume of tissue (voxel) by the three following equations that describe:

Table 2 Physiological models.

I — Tissue perfusion models — first-pass analysis[a]	
Deconvolution	
Axel	[1]
Ostergaard — Sorensen	[112]
Steepest slope method	
Miles	[5]
II — ''Permeability'' models[b]	
Models neglecting the tissue blood volume	
Tofts — Kermodes or Tofts-Kety, Brix1, Larsson	[6,7,24,158]
Patel	[113]
Models taking the tissue blood volume into account	
Without return	
Patlak, Miles, Shames — Brash	[20,26,114]
With return: Extended Kety or Tofts General Kinetic Model (GKM)	
Larsson	[159]
III — Complete models with exchanges — (perfusion and permeability)[b]	
Without return — (3 parameters)	
Cuenod — Pradel — de Bazelaire	[89,90]
With return — (4 parameters)	
Adiabatic approximation of tissue homogeneity (AATH)	
St Lawrence and Lee	[115]
Two-compartment exchange model	
Brix2	[116,117]
Comprehensive model: Cuenod — Balvay	[118,119]
2CX Sourbron — Buckley	[120,121]
Larsson	[122]
Distributed parameter model (DP model)	
Koh — Dennis Cheong — Bisdas	[123,124]
Physiologically based pharmacokinetic (PBPK) modelling	
Brochot — Bois	[125]

[a] For models studying tissue blood flow (perfusion), a high temporal resolution often requires the use of a delay parameter (Bolus Arrival Time) to account for the travel time of blood between the artery where the AIF is measured and the tissue.
[b] ''Permeability'' models are only valid if the temporal resolution is low, acquisition sufficiently long (Table 3) and if permeability is the main phenomenon.

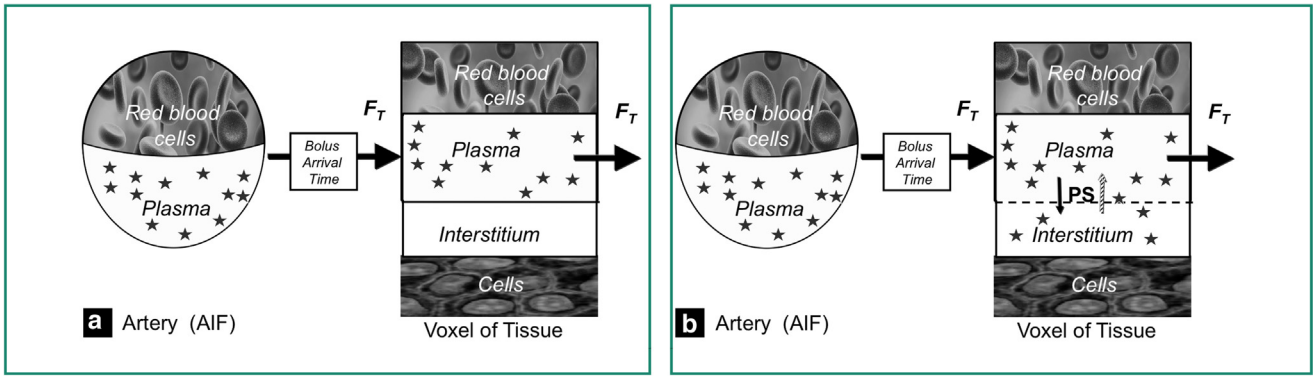

Figure 8. Schematic representation of the interaction between the different compartments of a voxel. Exchanges are characterized by transfer constants: transfer constant between the artery (arterial input function) and tissue (F_T) and transfer constants between the plasma and interstitium ($P \times S$) (leakage of plasma into the interstitium and return from the interstitium to the plasma): a: in the case of an impermeable capillary wall; b: in the case of a permeable capillary wall. These diagrams, constructed from Fig. 3, make it possible to pose the equations governing the interaction between the different compartments. The contrast agent has no access to the compartments occupied by red blood cells and cells but their volumes must be taken into account as they are contained in the voxels measured by cross-sectional imaging. A delay (Bolus Arrival Time) should be introduced to take into account the time lag between the passage of the bolus in the artery where the measurement is made and the tissue.

the quantity of contrast agent in the voxel of tissue:

$$q_t = q_p + q_e + q_{BC} + q_{cell}$$

the change in the quantity of contrast agent in the voxel plasma:

$$d_{qp}/d_t = (F_{Tp} \times q_{ap}) - (F_{Tp} \times q_{tp}/v_{tp}) - (PS \times q_{tp}/v_{tp}) + (PS \times q_e/v_e)$$

the change in the quantity of contrast agent in the voxel interstitium:

$$d_{qe}/d_t = (PS \times q_{tp}/v_{tp}) - (PS \times q_{ie}/v_e)$$

where: q_t is the quantity of contrast agent contained at time t in one voxel of tissue, q_{tp} the quantity of contrast agent contained in the plasma present in the voxel, q_e the quantity contained in the voxel interstitium, q_{BCr} and q_{cell} the quantities contained in the formed elements of the blood and tissue cells (given that these quantities are zero for the contrast agents used), q_{ap} the quantity of contrast agent in the plasma contained in one voxel of arterial blood, F_{Tp} represents the plasma flow rate entering and exiting a voxel, PS represents the transcapillary leakage factor in the form of the permeability—surface area product contained in a voxel (the PS values of leaving the capillary and return in the capillary are assumed to be equal in order to resolve the equation system), v_{tp} is the volume of plasma contained in the voxel and v_e the volume of the voxel interstitium.

By using computers, this equation system can be solved for the tissue enhancement curve by taking into account the arterial input function (AIF). The computer tests different values of the desired parameters in order to obtain the best fit of the curve modelled with the actual measured tissue enhancement curve using techniques to minimise differences (least squares methods).

It is important to note (Table 3) that only certain microcirculatory parameters may be determined depending on the measurement conditions (temporal resolution and total acquisition time). It is therefore important to adapt the selected model to the measurement conditions. Conversely, it is important to design the acquisition protocol based on the desired parameters to be measured. Table 3 provides a guide for these two tasks. All parameters become accessible with the highest temporal resolution and longest total acquisition time (box on the top right of the table) (if the signal to noise ratio is sufficient and if the difference between the tissue perfusion value and PS is sufficient) with complete four-parameter models including perfusion and permeability. Measurements of tissue blood volume and capillary permeability only require a relatively low frame rate for acquisition of 3D volumes with ''extended Kety-GKM'' type models if the acquisition is long (right bottom box) [159], or ''Patlak type'' models if the acquisition is a bit shorter (middle bottom box) [20,26,114]. On the contrary, measurement of tissue blood flow requires a rapid acquisition rate reducing the volume of tissue that can be analyzed with so-called ''first-pass'' models (top left box) [5].

The rational choice of model [118,129,130] may require curve fitting quality criteria [118,131,132]. Indeed, pitfalls include the use of an over-parameterized model providing values for parameters whose information is not contained in the data or the use of under-parameterized models that corrupt the measured parameters by trying to incorporate the information contained in the data, but not taken into account by the too simplistic model.

Arterial input function. Although different teams all agree that the quantitative analysis of the microcirculation requires knowledge of the kinetics of the contrast agent in the afferent artery to the tissue of interest (AIF) in order to fit the models, the methods of collecting this AIF vary considerably. There is a debate about whether the AIF should be measured from each examination for a given patient, or if an average AIF (population AIF) can be used interchangeably to fit all patients. Individual measurements have the advantage

Table 3 Accessible microvascular parameters according to acquisition conditions. The chosen model for fitting the enhancement curve takes into account the arterial input function (AIF) and must be adapted to the acquisition conditions. The complete models may be used to extract all the parameters, but they can only be applied for the case shown in the top right box when acquisition is achieved with a high temporal resolution (typically less than one acquisition every 5 seconds) over a long total duration (typically greater than 5 minutes). The evaluation of measurable parameters in the data can be achieved by using quality criteria for fitting the enhancement curve by different models [118,130].

Acquisition length Frequency	Short 60 s	Intermediate	Long ≥ 600 s
High 1—3 s	FT v_b MTT (first passage) □ □	FT v_b MTT PS □	FT v_b MTT PS v_e (complete model)
Intermediate		v_b □ PS □ (Patlak)	v_b □ PS v_e (extended Tofts-Kety)
Low 30—60 s			

s: second; MTT: mean transit time; S: fractional blood volume; PS: Permeability—surface product; v_e: fractional interstitial volume; the empty boxes represent the missing parameters that can not been estimated using the acquisition parameters.

that they provide precise blood kinetics taking into accounts each patient's hemodynamic parameters, but they are hampered by the fact that it is difficult to accurately measure the AIF. If the measurement is poor, it can lead to a significant error in the fitted parameters and induce variability in the results. Positioning a ROI on the afferent artery, for example, is not always feasible: there may not be a visible artery in the investigated area, as for example during single-slice ultrasound, or the artery can be too small to contain an ROI without causing a partial volume effect (leading to an artificial reduction in the first passage peak height and area under the arterial enhancement curve).

AIF measurement in a large artery. Given the fact that the arterial blood from the heart is distributed homogeneously throughout the arterial tree, a large artery (such as the aorta or the iliac or the carotid artery) can be used to obtain a proxy of the AIF for the tissue of interest. As there is a delay between the time of passage of the bolus in the artery where the measurement of the AIF is made and its arrival in the afferent arteriole of the tissue, a parameter called the Bolus Arriving Time (BAT) must be added in models using high temporal resolutions (Fig. 8). Four-parameter models thereby become 5-parameter models. There are also very slight changes in contrast agent kinetics between a large vessel and a more distal artery; as it is difficult to correct for these differences they are usually ignored.

For studies on drugs, it is recommended that the individual AIF is measured [126]. However, given the requirement for high spatial and temporal resolution, the reliability of the AIF measured for the target organ must be studied before designing the imaging protocol [133]; it is recommended to perform the same measurements twice on a sample of healthy subjects [134] to assess the reproducibility of the analyses.

AIF measurement in a small artery. If only a small artery is available, as in the brain, correction techniques for partial volume effects can be used. One technique is to use a multiplicative factor so that the area under the curve of the corrected AIF is equal to the area under the curve of a vein (as veins have a larger volume than arteries, there is a lower risk of partial volume) [135]. As the total amount of contrast agent entering by the arteries is equivalent to that exiting in the venous system, the areas under the arterial and venous curves must be equal.

Motion artefacts can also make it difficult to obtain a reliable measurement of AIF in a small artery.

The choice of the reference artery can be made by the operator or be assisted by semi-automatic techniques highlighting the most representative pixels of the AIF [136—138].

Population AIF. If no vessel is available, a mean AIF corresponding to an average value obtained in a population can be used [139,140]. This is the technique conventionally used in the Tofts model. Although this technique is simple, in principle it must be calibrated for the specific injection mode used and does not take into account individual variability among patients, which can be very large (morphology and total blood distribution volume, cardiac output, renal function, etc.) [141]. Although it is impossible in this case to compare the individual results of two patients, populations can still be compared (using statistical averages) and comparisons between two areas of tissue in the same patient are also possible, as modelling is carried out with the same AIF (albeit imperfect), so there is a normalization effect.

An intermediate approach is to use a population AIF and to correct these using individual values measured in a small artery [13,142].

Reference tissue. Certain authors have proposed using the enhancement kinetics of a reference tissue visible in the scanned region (e.g. muscle) with microcirculation parameters that are assumed to be known, in order to deduce an AIF and perform quantitative analysis even if no artery is available [143]. This technique, called the ''Reference Region Model'' (RRM) is limited by the low signal

to noise ratio obtained in weakly perfused tissues such as muscle, but it has been shown that in some cases the results are more reliable than with a poor individual AIF [144].

Specific case of the liver: double arterial and portal inflow. In the liver, the double blood supply by the hepatic artery and portal vein must be taken into account. It has been shown that a weighted sum of the two input kinetics could be used to model the hepatic microcirculation and determine the respective role of the two supplies expressed by the hepatic perfusion index HPI [50,145,146]. It is easy to measure the AIF in the descending aorta, but the difficulty lies in obtaining a reliable measurement of the portal entry function by positioning a region of interest in the portal vein, which undergoes numerous movements. Therefore motion correction is mandatory.

Analysis on a ROI, groups of voxels, and individual voxels plan

Results may be analyzed and expressed in different ways [147]: the analysis can be made for large ROIs drawn by the observer, on groups of pixels automatically identified according to specific criteria (clusters), or voxel-by-voxel. This choice depends on the application and computational tools available.

Analysis of global regions of interest. Large ROI analysis is simple and has the advantage of grouping many voxels together. This gives a high signal to noise ratio and makes the analysis of enhancement curves more robust. It provides a single value per ROI that can easily be noted in a report and simplifies the statistical analysis. Modelling with software is performed very rapidly. The main drawback of this approach, however, is that it erases all the specific data by averaging voxels that may have very different behaviors (e.g. voxels containing avascular necrosis and richly vascularized voxels) so that modelling gives an enhancement curve which may not have any real physiological basis as it is a mixture of different behaviors.

Voxel-by-voxel analysis: parametric mapping. On the contrary, voxel-by-voxel analysis focusing on each individual voxel of tissue, shows up any local heterogeneities and therefore may highlight hyperpermable or hypervascular areas (hot spots). This analysis requires much greater computing resources and a longer computation time, and in particular, if the signal to noise ratio is not sufficient at the level of an individual voxel because of its small size, the quality of fitting to models is compromised [148] and therefore unreliable.

The large amount of data obtained is represented by parametric colour images (one image per parameter), providing a summary of the dynamic series that is easily interpreted by the radiologist. On the other hand, numerical synthesis of the results is more difficult as each voxel has a series of values for each parameter. It is then possible to draw (a priori or a posteriori) ROIs that again give a mean value or use histograms that can be compared, for example, before and after treatment [149,150]. The choice of voxel-by-voxel analysis is currently driven by the interest in the study of tumor heterogeneity [151—153].

Analysis on homogeneous voxel clusters. An intermediate strategy between the analysis of global ROIs and voxel-by-voxel analysis is to group voxels together in clusters with either similar structural and signal characteristics before contrast injection [154], or a similar enhancement [155—157]. The use of these homogeneous voxel clusters provides high signal to noise ratios and consistent behaviors that make sense from a physiological point of view [94,155]. This method provides a concise view of areas with different physiological characteristics.

Quality of results and interchangeability of methods

Plan the different ways that data are acquired, analyzed and expressed should be taken into account [158,159]. For routine clinical analysis, where functional imaging of the microcirculation is only used to complement the morphological analysis — for example to assess the volume of ischemic territory or the absence of ''revascularization'' after tumor surgery — visual analysis of even rudimentary parametric maps or simple enhancement curves may be sufficient, even if the acquisitions are obtained with different imaging devices. On the contrary, if the goal is to extract quantitative values for use as imaging biomarkers to assess the efficacy of a new drug or accurately monitor the progression of a disease and control its management, it is important that the measurement method is accurate, i.e. reliable (giving a similar result when a parameter is measured several times) and correct (giving a value close to the true result). The use of analytical methods using different algorithms on the same set of data has been shown to yield different results [32]. Because of the current lack of a consensus and equivalence between methods, it is important to only compare the results obtained with a strictly identical acquisition and data analysis protocol. This improves the reproducibility of results, allowing for comparison, rather than their absolute accuracy.

For this purpose, the RSNA has set up a Quantitative Imaging Biomarker Alliance committee called the QIBA DCE-MRI Technical Committee whose task is to define the basic standards for DCE-MRI measurements and quality controls that provide reliable Ktrans and initial AUC values across imaging platforms, clinical sites, and time.

Conclusion

Imaging, as well as providing very specific morphological information on tissues, can also provide functional information about the microcirculation in many diseases (ischemia, tumors, inflammation, etc.) by analyzing the enhancement kinetics induced by the dynamic injection of a contrast agent.

Analysis of these kinetics can be visual, qualitative, or better, quantitative by providing microcirculation parameters that can be used as imaging biomarkers. This analysis requires dedicated software that must be adapted to the type of data collected. It is also important that the acquisition protocol is appropriate to the tissue examined, the desired parameters to be measured and the analysis mode.

In clinical practice, the functional information obtained by DCE-imaging is increasingly associated with morphological criteria for diagnosis (detection and characterization), prognostic evaluation (aggressiveness, viability) and monitoring of treatment of various diseases (efficacy, treatment adjustment).

TAKE-HOME MESSAGES

- DCE-imaging techniques (DCE-CT, DCE-MRI and DCE-US) may be used to assess the tissue microcirculation parameters.
- These parameters can be used as imaging biomarkers for diagnosis, prognosis or monitoring during treatment.
- The microcirculation parameters are the tissue perfusion flow, blood volume fraction, mean transit time, capillary permeability per unit tissue volume and interstitial volume fraction. The latter two parameters cannot be estimated by DCE-US.
- The parameter Ktrans, used to characterize the behavior of the contrast agent, is robust but does not correspond to an actual physiological parameter and varies with the acquisition protocol.
- The measurement of the arterial input function (AIF) is required to access quantitative parameters.

Disclosure of interest

The authors declare that they have no conflicts of interest concerning this article.

References

[1] Axel L. Cerebral blood flow determination by rapid-sequence computed tomography: theoretical analysis. Radiology 1980;137:679—86.

[2] Le Bihan D, Breton E, Lallemand D, Grenier P, Cabanis E, Laval-Jeantet M. MR imaging of intravoxel incoherent motions: application to diffusion and perfusion in neurologic disorders. Radiology 1986;161:401—7.

[3] Detre JA, Eskey CJ, Koretsky AP. Measurement of cerebral blood flow in rat brain by 19F-NMR detection of trifluoromethane washout. Magn Reson Med 1990;15:45—57.

[4] Schmiedl U, Brasch RC, Ogan MD, Moseley ME. Albumin labeled with Gd-DTPA. An intravascular contrast-enhancing agent for magnetic resonance blood pool and perfusion imaging. Acta Radiol Suppl 1990;374:99—102.

[5] Miles KA. Measurement of tissue perfusion by dynamic computed tomography. Br J Radiol 1991;64:409—12.

[6] Tofts PS, Kermode AG. Blood-brain barrier permeability in multiple sclerosis using labelled DTPA with PET, CT and MRI. J Neurol Neurosurg Psychiatry 1989;52:1019—20.

[7] Larsson HB, Stubgaard M, Frederiksen JL, Jensen M, Henriksen O, Paulson OB. Quantitation of blood-brain barrier defect by magnetic resonance imaging and gadolinium-DTPA in patients with multiple sclerosis and brain tumors. Magn Reson Med 1990;16:117—31.

[8] Sahani DV, Kalva SP, Hamberg LM, Hahn PF, Willett CG, Saini S, et al. Assessing tumor perfusion and treatment response in rectal cancer with multisection CT: initial observations. Radiology 2005;234:785—92.

[9] Padhani AR, Hayes C, Assersohn L, Powles T, Makris A, Suckling J, et al. Prediction of clinicopathologic response of breast cancer to primary chemotherapy at contrast-enhanced MR imaging: initial clinical results. Radiology 2006;239:361—74.

[10] Morgan B, Utting JF, Higginson A, Thomas AL, Steward WP, Horsfield MA. A simple, reproducible method for monitoring the treatment of tumours using dynamic contrast-enhanced MR imaging. Br J Cancer 2006;94:1420—7.

[11] O'Connor JP, Jackson A, Parker GJ, Jayson GC. DCE-MRI biomarkers in the clinical evaluation of antiangiogenic and vascular disrupting agents. Br J Cancer 2007;96:189—95.

[12] Fournier LS, Oudard S, Thiam R, Trinquart L, Banu E, Medioni J, et al. Metastatic renal carcinoma: evaluation of antiangiogenic therapy with dynamic contrast-enhanced CT. Radiology 2010;256:511—8.

[13] de Bazelaire C, Calmon R, Thomassin I, Brunon C, Hamy AS, Fournier L, et al. Accuracy of perfusion MRI with high spatial but low temporal resolution to assess invasive breast cancer response to neoadjuvant chemotherapy: a retrospective study. BMC Cancer 2011;11:361.

[14] Yu HJ, Chen JH, Mehta RS, Nalcioglu O, Su MY. MRI measurements of tumor size and pharmacokinetic parameters as early predictors of response in breast cancer patients undergoing neoadjuvant anthracycline chemotherapy. J Magn Reson Imaging 2007;26:615—23.

[15] Jain RK, Duda DG, Willett CG, Sahani DV, Zhu AX, Loeffler JS, et al. Biomarkers of response and resistance to antiangiogenic therapy. Nat Rev Clin Oncol 2009;6:327—38.

[16] Kety SS, Schmidt CF. The nitrous oxide method for the quantitative determination of cerebral blood flow in man: theory, procedure and normal values. J Clin Invest 1948;27:476—83.

[17] Johnson JA, Wilson TA. A model for capillary exchange. Am J Physiol 1966;210:1299—303.

[18] Jacquez JA. Compartmental analysis in biology and medicine. Ann Arbor: The University of Michigan Press; 1985.

[19] Kety SS. Regional cerebral blood flow: estimation by means of nonmetabolized diffusible tracers — an overview. Semin Nucl Med 1985;15:324—8.

[20] Patlak CS, Blasberg RG, Fenstermacher JD. Graphical evaluation of blood-to-brain transfer constants from multiple-time uptake data. J Cereb Blood Flow Metab 1983;3:1—7.

[21] Meier P, Zierler KL. On the theory of the indicator-dilution method for measurement of blood flow and volume. J Appl Physiol 1954;6:731—44.

[22] Villringer A, Rosen BR, Belliveau JW, Ackerman JL, Lauffer RB, Buxton RB, et al. Dynamic imaging with lanthanide chelates in normal brain: contrast due to magnetic susceptibility effects. Magn Reson Med 1988;6:164—74.

[23] Tofts PS, Brix G, Buckley DL, Evelhoch JL, Henderson E, Knopp MV, et al. Estimating kinetic parameters from dynamic contrast-enhanced T(1)-weighted MRI of a diffusable tracer: standardized quantities and symbols. J Magn Reson Imaging 1999;10:223—32.

[24] Brix G, Semmler W, Port R, Schad LR, Layer G, Lorenz WJ. Pharmacokinetic parameters in CNS Gd-DTPA enhanced MR imaging. J Comput Assist Tomogr 1991;15:621—8.

[25] Burstein D, Taratuta E, Manning WJ. Factors in myocardial ''perfusion'' imaging with ultrafast MRI and Gd-DTPA administration. Magn Reson Med 1991;20:299—305.

[26] Shames DM, Kuwatsuru R, Vexler V, Muhler A, Brasch RC. Measurement of capillary permeability to macromolecules by dynamic magnetic resonance imaging: a quantitative noninvasive technique. Magn Reson Med 1993;29:616—22.

[27] Donahue KM, Weisskoff RM, Parmelee DJ, Callahan RJ, Wilkinson RA, Mandeville JB, et al. Dynamic Gd-DTPA enhanced MRI measurement of tissue cell volume fraction. Magn Reson Med 1995;34:423—32.

[28] Ostergaard L, Weisskoff RM, Chesler DA, Gyldensted C, Rosen BR. High resolution measurement of cerebral blood flow using intravascular tracer bolus passages. Part I: mathematical approach and statistical analysis. Magn Reson Med 1996;36:715—25.

[29] Parker GJ, Tofts PS. Pharmacokinetic analysis of neoplasms using contrast-enhanced dynamic magnetic resonance imaging. Top Magn Reson Imaging 1999;10:130—42.
[30] Miles KA, Lee TY, Goh V, Klotz E, Cuenod C, Bisdas S, et al. Current status and guidelines for the assessment of tumour vascular support with dynamic contrast-enhanced computed tomography. Eur Radiol 2012;22:1430—41.
[31] Bisdas S, Foo CZ, Thng CH, Vogl TJ, Koh TS. Optimization of perfusion CT protocol for imaging of extracranial head and neck tumors. J Digit Imaging 2008;22(5):437—48.
[32] Goh V, Halligan S, Bartram CI. Quantitative tumor perfusion assessment with multidetector CT: are measurements from two commercial software packages interchangeable? Radiology 2007;242:777—82.
[33] Petralia G, Bonello L, Priolo F, Summers P, Bellomi M. Breast MR with special focus on DW-MRI and DCE-MRI. Cancer Imaging 2011;11:76—90.
[34] Lassau N, Chapotot L, Benatsou B, Vilgrain V, Kind M, Lacroix J, et al. Standardization of dynamic contrast-enhanced ultrasound for the evaluation of antiangiogenic therapies: the French multicenter Support for Innovative and Expensive Techniques Study. Invest Radiol 2012;47:711—6.
[35] Folkman J. Tumor angiogenesis: therapeutic implications. N Engl J Med 1971;285:1182—6.
[36] Brasch R, Pham C, Shames D, Roberts T, van Dijke K, van Bruggen N, et al. Assessing tumor angiogenesis using macromolecular MR imaging contrast media. J Magn Reson Imaging 1997;7:68—74.
[37] Miles KA. Tumour angiogenesis and its relation to contrast enhancement on computed tomography: a review. Eur J Radiol 1999;30:198—205.
[38] Neeman M. Preclinical MRI experience in imaging angiogenesis. Cancer Metastasis Rev 2000;19:39—43.
[39] Padhani AR, Neeman M. Challenges for imaging angiogenesis. Br J Radiol 2001;74:886—90.
[40] Li KC. Angiogenesis imaging in the post-genomic era. Br J Radiol 2003;76(Spec nº 1):S1—2.
[41] McDonald DM, Choyke PL. Imaging of angiogenesis: from microscope to clinic. Nat Med 2003;9:713—25.
[42] Choyke PL. Contrast agents for imaging tumor angiogenesis: is bigger better? Radiology 2005;235:1—2.
[43] Cuenod CA, Fournier L, Balvay D, Guinebretiere JM. Tumor angiogenesis: pathophysiology and implications for contrast-enhanced MRI and CT assessment. Abdom Imaging 2006;31:188—93.
[44] Daldrup-Link HE, Simon GH, Brasch RC. Imaging of tumor angiogenesis: current approaches and future prospects. Curr Pharm Des 2006;12:2661—72.
[45] Fritz-Hansen T, Rostrup E, Sondergaard L, Ring PB, Amtorp O, Larsson HB. Capillary transfer constant of Gd-DTPA in the myocardium at rest and during vasodilation assessed by MRI. Magn Reson Med 1998;40:922—9.
[46] Lee R, Cheung RT, Hung KN, Au-Yeung KM, Leong LL, Chan FL, et al. Use of CT perfusion to differentiate between brain tumour and cerebral infarction. Cerebrovasc Dis 2004;18:77—83.
[47] Wintermark M. Brain perfusion-CT in acute stroke patients. Eur Radiol 2005;15(Suppl 4):D28—31.
[48] Choyke PL, Kobayashi H. Functional magnetic resonance imaging of the kidney using macromolecular contrast agents. Abdom Imaging 2006;31:224—31.
[49] Miles KA, Leggett DA, Bennett GA. CT derived Patlak images of the human kidney. Br J Radiol 1999;72:153—8.
[50] Cuenod C, Leconte I, Siauve N, Resten A, Dromain C, Poulet B, et al. Early changes in liver perfusion caused by occult metastases in rats: detection with quantitative CT. Radiology 2001;218:556—61.
[51] Knopp MV, Brix G, Junkermann HJ, Sinn HP. MR mammography with pharmacokinetic mapping for monitoring of breast cancer treatment during neoadjuvant therapy. Magn Reson Imaging Clin N Am 1994;2:633—58.
[52] Thomassin-Naggara I, Bazot M, Darai E, Callard P, Thomassin J, Cuenod CA. Epithelial ovarian tumors: value of dynamic contrast-enhanced MR imaging and correlation with tumor angiogenesis. Radiology 2008;248:148—59.
[53] Hermans R, Lambin P, Van der Goten A, Van den Bogaert W, Verbist B, Weltens C, et al. Tumoural perfusion as measured by dynamic computed tomography in head and neck carcinoma. Radiother Oncol 1999;53:105—11.
[54] Kauczor HU, Kreitner KF. Contrast-enhanced MRI of the lung. Eur J Radiol 2000;34:196—207.
[55] Kiessling F, Boese J, Corvinus C, Ederle JR, Zuna I, Schoenberg SO, et al. Perfusion CT in patients with advanced bronchial carcinomas: a novel chance for characterization and treatment monitoring? Eur Radiol 2004;14:1226—33.
[56] Dyke JP, Aaron RK. Noninvasive methods of measuring bone blood perfusion. Ann N Y Acad Sci 2010;1192:95—102.
[57] Lin C, Luciani A, Belhadj K, Deux JF, Kuhnowski F, Maatouk M, et al. Multiple myeloma treatment response assessment with whole-body dynamic contrast-enhanced MR imaging. Radiology 2010;254:521—31.
[58] Del Vescovo R, Sansoni I, Caviglia R, Ribolsi M, Perrone G, Leoncini E, et al. Dynamic contrast-enhanced magnetic resonance imaging of the terminal ileum: differentiation of activity of Crohn's disease. Abdom Imaging 2008;33:417—24.
[59] Bali MA, Metens T, Denolin V, Delhaye M, Demetter P, Closset J, et al. Tumoral and nontumoral pancreas: correlation between quantitative dynamic contrast-enhanced MR imaging and histopathologic parameters. Radiology 2011;261:456—66.
[60] Salomon LJ, Siauve N, Balvay D, Cuénod CA, Vayssettes C, Luciani A, et al. Placental perfusion MR imaging with contrast agents in a mouse model. Radiology 2005;235:73—80.
[61] Franiel T, Hamm B, Hricak H. Dynamic contrast-enhanced magnetic resonance imaging and pharmacokinetic models in prostate cancer. Eur Radiol 2011;21:616—26.
[62] Hanna SL, Reddick WE, Parham DM, Gronemeyer SA, Taylor JS, Fletcher BD. Automated pixel-by-pixel mapping of dynamic contrast-enhanced MR images for evaluation of osteosarcoma response to chemotherapy: preliminary results. J Magn Reson Imaging 1993;3:849—53.
[63] O'Connor JP, Tofts PS, Miles KA, Parkes LM, Thompson G, Jackson A. Dynamic contrast-enhanced imaging techniques: CT and MRI. Br J Radiol 2011;84(Spec nº 2):S112—20.
[64] Sourbron SP, Buckley DL. On the scope and interpretation of the Tofts models for DCE-MRI. Magn Reson Med 2011;66:735—45.
[65] Stern MD, Lappe DL, Bowen PD, Chimosky JE, Holloway Jr GA, Keiser HR, et al. Continuous measurement of tissue blood flow by laser-Doppler spectroscopy. Am J Physiol 1977;232:H441—8.
[66] McDonald DM, Baluk P. Significance of blood vessel leakiness in cancer. Cancer Res 2002;62:5381—5.
[67] Faye N, Fournier L, Balvay D, Taillieu F, Cuenod C, Siauve N, et al. Dynamic contrast-enhanced optical imaging of capillary leakage. Technol Cancer Res Treat 2011;10:49—57.
[68] Itai Y, Ohtomo K, Kokubo T, Yamauchi T, Minami M, Yashiro N, et al. CT of hepatic masses: significance of prolonged and delayed enhancement. AJR Am J Roentgenol 1986;146:729—33.
[69] Mandeville HC, Ng QS, Daley FM, Barber PR, Pierce G, Finch J, et al. Operable non-small cell lung cancer: correlation of volumetric helical dynamic contrast-enhanced CT parameters with immunohistochemical markers of tumor hypoxia. Radiology 2012;264:581—9.

[70] Thieme SF, Becker CR, Hacker M, Nikolaou K, Reiser MF, Johnson TR. Dual energy CT for the assessment of lung perfusion — correlation to scintigraphy. Eur J Radiol 2008;68(3):369—74.
[71] Goh V, Dattani M, Farwell J, Shekhdar J, Tam E, Patel S, et al. Radiation dose from volumetric helical perfusion CT of the thorax, abdomen or pelvis. Eur Radiol 2011;21:974—81.
[72] Lassau N, Koscielny S, Opolon P, De Baere T, Peronneau P, Leclere J, et al. Evaluation of contrast-enhanced color Doppler ultrasound for the quantification of angiogenesis in vivo. Invest Radiol 2001;36:50—5.
[73] Williams R, Hudson JM, Lloyd BA, Sureshkumar AR, Lueck G, Milot L, et al. Dynamic microbubble contrast-enhanced US to measure tumor response to targeted therapy: a proposed clinical protocol with results from renal cell carcinoma patients receiving antiangiogenic therapy. Radiology 2011;260:581—90.
[74] van Gelderen P, de Zwart JA, Duyn JH. Pittfalls of MRI measurement of white matter perfusion based on arterial spin labeling. Magn Reson Med 2008;59:788—95.
[75] Detre JA, Zhang W, Roberts DA, Silva AC, Williams DS, Grandis DJ, et al. Tissue specific perfusion imaging using arterial spin labeling. NMR Biomed 1994;7:75—82.
[76] St Lawrence KS, Owen D, Wang DJ. A two-stage approach for measuring vascular water exchange and arterial transit time by diffusion-weighted perfusion MRI. Magn Reson Med 2012;67:1275—84.
[77] Kwong KK, Belliveau JW, Chesler DA, Goldberg IE, Weisskoff RM, Poncelet BP, et al. Dynamic magnetic resonance imaging of human brain activity during primary sensory stimulation. Proc Natl Acad Sci U S A 1992;89:5675—9.
[78] Gillis P, Peto S, Moiny F, Mispelter J, Cuenod CA. Proton transverse nuclear magnetic relaxation in oxidized blood: a numerical approach. Magn Reson Med 1995;33:93—100.
[79] Towse TF, Slade JM, Ambrose JA, DeLano MC, Meyer RA. Quantitative analysis of the postcontractile blood-oxygenation-level-dependent (BOLD) effect in skeletal muscle. J Appl Physiol 2011;111:27—39.
[80] Hunold P, Schlosser T, Vogt FM, Eggebrecht H, Schmermund A, Bruder O, et al. Myocardial late enhancement in contrast-enhanced cardiac MRI: distinction between infarction scar and non-infarction-related disease. AJR Am J Roentgenol 2005;184:1420—6.
[81] Thomassin-Naggara I, Darai E, Nassar-Slaba J, Cortez A, Marsault C, Bazot M. Value of dynamic enhanced magnetic resonance imaging for distinguishing between ovarian fibroma and subserous uterine leiomyoma. J Comput Assist Tomogr 2007;31:236—42.
[82] Ogan MD, Schmiedl U, Moseley ME, Grodd W, Paajanen H, Brasch RC. Albumin labeled with Gd-DTPA. An intravascular contrast-enhancing agent for magnetic resonance blood pool imaging: preparation and characterization. Invest Radiol 1987;22:665—71.
[83] Aicher KP, Dupon JW, White DL, Aukerman SL, Moseley ME, Juster R, et al. Contrast-enhanced magnetic resonance imaging of tumor-bearing mice treated with human recombinant tumor necrosis factor alpha. Cancer Res 1990;50:7376—81.
[84] Vexler VS, Clement O, Schmitt-Willich H, Brasch RC. Effect of varying the molecular weight of the MR contrast agent Gd-DTPA-polylysine on blood pharmacokinetics and enhancement patterns. J Magn Reson Imaging 1994;4:381—8.
[85] Clement O, Vuillemin-Bodaghi V, Cuenod CA, Siauve N, Blustajn J, Frija G. Quantification of liver capillary permeability using a macromolecular contrast agent for magnetic resonance imaging. Acad Radiol 1996;3(Suppl. 2):S342—3.
[86] Jerosch-Herold M, Wilke N, Wang Y, Gong GR, Mansoor AM, Huang H, et al. Direct comparison of an intravascular and an extracellular contrast agent for quantification of myocardial perfusion. Int J Card Imaging 1999;15:453—64.
[87] Daldrup-Link HE, Shames DM, Wendland M, Mühler A, Gossmann A, Rosenau W, et al. Comparison of Gadomer-17 and gadopentetate dimeglumine for differentiation of benign from malignant breast tumors with MR imaging. Acad Radiol 2000;7:934—44.
[88] Turetschek K, Floyd E, Shames DM, Roberts TP, Preda A, Novikov V, et al. Assessment of a rapid clearance blood pool MR contrast medium (P792) for assays of microvascular characteristics in experimental breast tumors with correlations to histopathology. Magn Reson Med 2001;45:880—6.
[89] Pradel C, Siauve N, Bruneteau G, Clement O, de Bazelaire C, Frouin F, et al. Reduced capillary perfusion and permeability in human tumour xenografts treated with the VEGF signalling inhibitor ZD4190: an in vivo assessment using dynamic MR imaging and macromolecular contrast media. Magn Reson Imaging 2003;21:845—51.
[90] de Bazelaire C, Siauve N, Fournier L, Frouin F, Robert P, Clement O, et al. Comprehensive model for simultaneous MRI determination of perfusion and permeability using a blood-pool agent in rats rhabdomyosarcoma. Eur Radiol 2005;15:2497—505.
[91] Canet E, Revel D, Forrat R, Baldy-Porcher C, de Lorgeril M, Sebbag L, et al. Superparamagnetic iron oxide particles and positive enhancement for myocardial perfusion studies assessed by subsecond T1-weighted MRI. Magn Reson Imaging 1993;11:1139—45.
[92] Trillaud H, Grenier N, Degreze P, Louail C, Chambon C, Franconi JM. First-pass evaluation of renal perfusion with TurboFLASH MR imaging and superparamagnetic iron oxide particles. J Magn Reson Imaging 1993;3:83—91.
[93] Morell A, Ahlstrom H, Schoenberg SO, Abildgaard A, Bock M, Bjornerud A. Quantitative renal cortical perfusion in human subjects with magnetic resonance imaging using iron-oxide nanoparticles: influence of T1 shortening. Acta Radiol 2008;49:955—62.
[94] Kachenoura N, Cluzel P, Frouin F, Toledano D, Grenier P, Cuenod CA, et al. Evaluation of an edge-based registration method: application to magnetic resonance first-pass myocardial perfusion data. Magn Reson Imaging 2011;29:853—60.
[95] Xue H, Guehring J, Srinivasan L, Zuehlsdorff S, Saddi K, Chefdhotel C, et al. Evaluation of rigid and non-rigid motion compensation of cardiac perfusion MRI. Med Image Comput Comput Assist Interv 2008;11:35—43.
[96] Buonaccorsi GA, O'Connor JP, Caunce A, Roberts C, Cheung S, Watson Y, et al. Tracer kinetic model-driven registration for dynamic contrast-enhanced MRI time-series data. Magn Reson Med 2007;58:1010—9.
[97] Hachama M, Desolneux A, Cuenod CA, Richard FJ. A classifying registration technique for the estimation of enhancement curves of DCE-CT scan sequences. Med Image Anal 2010;14:185—94.
[98] Balvay D, Kachenoura N, Espinoza S, Thomassin-Naggara I, Fournier LS, Clement O, et al. Signal-to-noise ratio improvement in dynamic contrast-enhanced CT and MR imaging with automated principal component analysis filtering. Radiology 2011;258:435—45.
[99] Bellamy DD, Pereira RS, McKenzie CA, Prato FS, Drost DJ, Sykes J, et al. Gd-DTPA bolus tracking in the myocardium using T1 fast acquisition relaxation mapping (T1 FARM). Magn Reson Med 2001;46:555—64.
[100] Treier R, Steingoetter A, Fried M, Schwizer W, Boesiger P. Optimized and combined T1 and B1 mapping technique for fast and accurate T1 quantification in contrast-enhanced abdominal MRI. Magn Reson Med 2007;57:568—76.
[101] Taheri S, Gasparovic C, Shah NJ, Rosenberg GA. Quantitative measurement of blood-brain barrier permeability in human using dynamic contrast-enhanced MRI with fast T1 mapping. Magn Reson Med 2011;65:1036—42.

[102] Utz W, Niendorf T, Wassmuth R, Messroghli D, Dietz R, Schulz-Menger J. Contrast-dose relation in first-pass myocardial MR perfusion imaging. J Magn Reson Imaging 2007;25:1131—5.
[103] De Naeyer D, Verhulst J, Ceelen W, Segers P, De Deene Y, Verdonck P. Flip angle optimization for dynamic contrast-enhanced MRI-studies with spoiled gradient echo pulse sequences. Phys Med Biol 2011;56(16):5373—95.
[104] Zhang JL, Koh TS. On the selection of optimal flip angles for T1 mapping of breast tumors with dynamic contrast-enhanced magnetic resonance imaging. IEEE Trans Biomed Eng 2006;53:1209—14.
[105] Taillieu F, Salomon LJ, Siauve N, Clément O, Faye N, Balvay D, et al. Placental perfusion and permeability: simultaneous assessment with dual-echo contrast-enhanced MR imaging in mice. Radiology 2006;241:737—45.
[106] Schnall MD, Blume J, Bluemke DA, DeAngelis GA, DeBruhl N, Harms S, et al. Diagnostic architectural and dynamic features at breast MR imaging: multicenter study. Radiology 2006;238:42—53.
[107] Lavini C, de Jonge MC, van de Sande MG, Tak PP, Nederveen AJ, Maas M. Pixel-by-pixel analysis of DCE-MRI curve patterns and an illustration of its application to the imaging of the musculoskeletal system. Magn Reson Imaging 2007;25:604—12.
[108] Degani H, Gusis V, Weinstein D, Fields S, Strano S. Mapping pathophysiological features of breast tumors by MRI at high spatial resolution. Nat Med 1997;3:780—2.
[109] Furman-Haran E, Degani H. Parametric analysis of breast MRI. J Comput Assist Tomogr 2002;26:376—86.
[110] Thomassin-Naggara I, Darai E, Cuenod CA, Rouzier R, Callard P, Bazot M. Dynamic contrast-enhanced magnetic resonance imaging: a useful tool for characterizing ovarian epithelial tumors. J Magn Reson Imaging 2008;28:111—20.
[111] Roberts C, Issa B, Stone A, Jackson A, Waterton JC, Parker GJ. Comparative study into the robustness of compartmental modeling and model-free analysis in DCE-MRI studies. J Magn Reson Imaging 2006;23:554—63.
[112] Ostergaard L, Sorensen AG, Kwong KK, Weisskoff RM, Gyldensted C, Rosen BR. High resolution measurement of cerebral blood flow using intravascular tracer bolus passages. Part II: experimental comparison and preliminary results. Magn Reson Med 1996;36:726—36.
[113] Patel PP, Koppenhafer SL, Scholz TD. Measurement of kinetic perfusion parameters of gadoteridol in intact myocardium: effects of ischemia/reperfusion and coronary vasodilation. Magn Reson Imaging 1995;13:799—806.
[114] Miles KA, Kelley BB. CT measurements of capillary permeability within nodal masses: a potential technique for assessing the activity of lymphoma. Br J Radiol 1997;70:74—9.
[115] St Lawrence KS, Lee TY. An adiabatic approximation to the tissue homogeneity model for water exchange in the brain: I. Theoretical derivation. J Cereb Blood Flow Metab 1998;18:1365—77.
[116] Brix G, Bahner ML, Hoffmann U, Horvath A, Schreiber W. Regional blood flow, capillary permeability, and compartmental volumes: measurement with dynamic CT — initial experience. Radiology 1999;210:269—76.
[117] Dennis Cheong LH, Tchoyoson Lim CC, Koh TS. Dynamic contrast-enhanced CT of intracranial meningioma: comparison of distributed and compartmental tracer kinetic models — initial results. Radiology 2004;232:921—30.
[118] Balvay D, Frouin F, Calmon G, Bessoud B, Kahn E, Siauve N, et al. New criteria for assessing fit quality in dynamic contrast-enhanced T1-weighted MRI for perfusion and permeability imaging. Magn Reson Med 2005;54:868—77.
[119] Thomassin-Naggara I, Balvay D, Cuenod CA, Darai E, Marsault C, Bazot M. Dynamic contrast-enhanced MR imaging to assess physiologic variations of myometrial perfusion. Eur Radiol 2010;20(4):984—94.
[120] Sourbron S, Ingrisch M, Siefert A, Reiser M, Herrmann K. Quantification of cerebral blood flow, cerebral blood volume, and blood-brain-barrier leakage with DCE-MRI. Magn Reson Med 2009;62:205—17.
[121] Donaldson SB, West CM, Davidson SE, Carrington BM, Hutchison G, Jones AP, et al. A comparison of tracer kinetic models for T1-weighted dynamic contrast-enhanced MRI: application in carcinoma of the cervix. Magn Reson Med 2010;63:691—700.
[122] Larsson HB, Courivaud F, Rostrup E, Hansen AE. Measurement of brain perfusion, blood volume, and blood-brain barrier permeability, using dynamic contrast-enhanced T(1)-weighted MRI at 3 tesla. Magn Reson Med 2009;62:1270—81.
[123] Koh TS, Cheong LH, Hou Z, Soh YC. A physiologic model of capillary-tissue exchange for dynamic contrast-enhanced imaging of tumor microcirculation. IEEE Trans Biomed Eng 2003;50:159—67.
[124] Dennis Cheong LH, Markus Tan CK, Koh TS, Tchoyoson Lim CC, Bisdas S. Functional imaging: dynamic contrast-enhanced ct using a distributed-parameter physiologic model for accessing stroke and intracranial tumor. Conf Proc IEEE Eng Med Biol Soc 2005;1:294—7.
[125] Brochot C, Bessoud B, Balvay D, Cuenod CA, Siauve N, Bois FY. Evaluation of antiangiogenic treatment effects on tumors' microcirculation by Bayesian physiological pharmacokinetic modeling and magnetic resonance imaging. Magn Reson Imaging 2006;24:1059—67.
[126] Leach MO, Brindle KM, Evelhoch JL, Griffiths JR, Horsman MR, Jackson A, et al. The assessment of antiangiogenic and antivascular therapies in early-stage clinical trials using magnetic resonance imaging: issues and recommendations. Br J Cancer 2005;92:1599—610.
[127] Tofts PS, Berkowitz B, Schnall MD. Quantitative analysis of dynamic Gd-DTPA enhancement in breast tumors using a permeability model. Magn Reson Med 1995;33:564—8.
[128] Sourbron SP, Buckley DL. Tracer kinetic modelling in MRI: estimating perfusion and capillary permeability. Phys Med Biol 2012;57:R1—33.
[129] Ewing JR, Brown SL, Lu M, Panda S, Ding G, Knight RA, et al. Model selection in magnetic resonance imaging measurements of vascular permeability: gadomer in a 9L model of rat cerebral tumor. J Cereb Blood Flow Metab 2006;26:310—20.
[130] Brix G, Zwick S, Kiessling F, Griebel J. Pharmacokinetic analysis of tissue microcirculation using nested models: multimodel inference and parameter identifiability. Med Phys 2009;36:2923—33.
[131] Balvay D, Troprès I, Billet R, Joubert A, Péoc'h M, Cuenod CA, et al. Mapping the zonal organization of tumor perfusion and permeability in a rat glioma model by using dynamic contrast-enhanced synchrotron radiation CT. Radiology 2009;250:692—702.
[132] Li X, Welch EB, Chakravarthy AB, Xu L, Arlinghaus LR, Farley J, et al. Statistical comparison of dynamic contrast-enhanced MRI pharmacokinetic models in human breast cancer. Magn Reson Med 2012;68:261—71.
[133] Cheng HL. Investigation and optimization of parameter accuracy in dynamic contrast-enhanced MRI. J Magn Reson Imaging 2008;28:736—43.
[134] Ashton E, Raunig D, Ng C, Kelcz F, McShane T, Evelhoch J. Scan-rescan variability in perfusion assessment of tumors in MRI using both model and data-derived arterial input functions. J Magn Reson Imaging 2008;28:791—6.
[135] van der Schaaf I, Vonken EJ, Waaijer A, Velthuis B, Quist M, van Osch T. Influence of partial volume on venous output and arterial input function. AJNR Am J Neuroradiol 2006;27:46—50.
[136] Calamante F, Morup M, Hansen LK. Defining a local arterial input function for perfusion MRI using independent component analysis. Magn Reson Med 2004;52:789—97.

[137] Mouridsen K, Christensen S, Gyldensted L, Ostergaard L. Automatic selection of arterial input function using cluster analysis. Magn Reson Med 2006;55:524—31.
[138] Ashton E, McShane T, Evelhoch J. Inter-operator variability in perfusion assessment of tumors in MRI using automated AIF detection. Med Image Comput Comput Assist Interv Int Conf Med Image Comput Comput Assist Interv 2005;8:451—8.
[139] Padhani AR. Functional MRI for anticancer therapy assessment. Eur J Cancer 2002;38:2116—27.
[140] Parker GJ, Roberts C, Macdonald A, Buonaccorsi GA, Cheung S, Buckley DL, et al. Experimentally-derived functional form for a population-averaged high-temporal-resolution arterial input function for dynamic contrast-enhanced MRI. Magn Reson Med 2006;56:993—1000.
[141] Port RE, Knopp MV, Brix G. Dynamic contrast-enhanced MRI using Gd-DTPA: interindividual variability of the arterial input function and consequences for the assessment of kinetics in tumors. Magn Reson Med 2001;45:1030—8.
[142] Kim SM, Haider MA, Milosevic M, Jaffray DA, Yeung IW. A method for patient dose reduction in dynamic contrast-enhanced CT study. Med Phys 2011;38:5094—103.
[143] Yankeelov TE, Luci JJ, Lepage M, Li R, Debusk L, Lin PC, et al. Quantitative pharmacokinetic analysis of DCE-MRI data without an arterial input function: a reference region model. Magn Reson Imaging 2005;23:519—29.
[144] Hsiao IT, Liao YP, Liu HL. Study of onset time-shift and injection duration in DCE-MRI: a comparison of a reference region model with the general kinetic model. NMR Biomed 2010;23:375—81.
[145] Materne R, Smith AM, Peeters F, Dehoux JP, Keyeux A, Horsmans Y, et al. Assessment of hepatic perfusion parameters with dynamic MRI. Magn Reson Med 2002;47:135—42.
[146] Koh TS, Thng CH, Lee PS, Hartono S, Rumpel H, Goh BC, et al. Hepatic metastases: in vivo assessment of perfusion parameters at dynamic contrast-enhanced MR imaging with dual-input two-compartment tracer kinetics model. Radiology 2008;249:307—20.
[147] d'Arcy JA, Collins DJ, Padhani AR, Walker-Samuel S, Suckling J, Leach MO. Informatics in radiology (infoRAD): Magnetic Resonance Imaging Workbench: analysis and visualization of dynamic contrast-enhanced MR imaging data. Radiographics 2006;26:621—32.
[148] Cuenod CA, Favetto B, Genon-Catalot V, Rozenholc Y, Samson A. Parameter estimation and change-point detection from dynamic contrast-enhanced MRI data using stochastic differential equations. Math Biosci 2011;233(1):68—76.
[149] Hayes C, Padhani AR, Leach MO. Assessing changes in tumour vascular function using dynamic contrast-enhanced magnetic resonance imaging. NMR Biomed 2002;15:154—63.
[150] Stoutjesdijk MJ, Veltman J, Huisman H, Karssemeijer N, Barentsz JO, Blickman JG, et al. Automated analysis of contrast enhancement in breast MRI lesions using mean shift clustering for ROI selection. J Magn Reson Imaging 2007;26:606—14.
[151] O'Connor JP, Rose CJ, Jackson A, Watson Y, Cheung S, Maders F, et al. DCE-MRI biomarkers of tumour heterogeneity predict CRC liver metastasis shrinkage following bevacizumab and FOLFOX-6. Br J Cancer 2011;105:139—45.
[152] Alic L, van Vliet M, van Dijke CF, Eggermont AM, Veenland JF, Niessen WJ. Heterogeneity in DCE-MRI parametric maps: a biomarker for treatment response? Phys Med Biol 2011;56:1601—16.
[153] Yang X, Knopp MV. Quantifying tumor vascular heterogeneity with dynamic contrast-enhanced magnetic resonance imaging: a review. J Biomed Biotechnol 2011;2011:732848.
[154] Kelm BM, Menze BH, Nix O, Zechmann CM, Hamprecht FA. Estimating kinetic parameter maps from dynamic contrast-enhanced MRI using spatial prior knowledge. IEEE Trans Med Imaging 2009;28:1534—47.
[155] Zöllner FG, Sance R, Rogelj P, Ledesma-Carbayo MJ, Rørvik J, Santos A, et al. Assessment of 3D DCE-MRI of the kidneys using non-rigid image registration and segmentation of voxel time courses. Comput Med Imaging Graph 2009;33:171—81.
[156] Eyal E, Badikhi D, Furman-Haran E, Kelcz F, Kirshenbaum KJ, Degani H. Principal component analysis of breast DCE-MRI adjusted with a model-based method. J Magn Reson Imaging 2009;30:989—98.
[157] Chen L, Choyke PL, Chan TH, Chi CY, Wang G, Wang Y. Tissue-specific compartmental analysis for dynamic contrast-enhanced MR imaging of complex tumors. IEEE Trans Med Imaging 2011;30:2044—58.
[158] Tofts PS. Modeling tracer kinetics in dynamic Gd-DTPA MR imaging. J Magn Reson Imaging 1997;7:91—101.
[159] Larsson HB, Fritz-Hansen T, Rostrup E, Sondergaard L, Ring P, Henriksen O. Myocardial perfusion modeling using MRI. Magn Reson Med 1996;35:716—26.